strain WILEY

Residual stresses in Cu matrix composite surface deposits after laser melt injection

Xingxing Zhang[1] | Joana R. Kornmeier[1] | Michael Hofmann[1] | Anika Langebeck[2] | Shadi Alameddin[3] | Renan Pereira Alessio[3] | Felix Fritzen[3] | Jeffrey R. Bunn[4] | Sandra Cabeza[5]

[1]Heinz Maier-Leibnitz Zentrum (MLZ), Technical University of Munich, Garching, Germany

[2]BIAS – Bremer Institut fuer angewandte Strahltechnik GmbH, Bremen, Germany

[3]Stuttgart Center for Simulation Science, Institute of Applied Mechanics (CE), University of Stuttgart, Stuttgart, Germany

[4]Neutron Scattering Science Division, Oak Ridge National Laboratory, Oak Ridge, Tennessee, USA

[5]Institut Laue-Langevin, Grenoble, France

Correspondence
Xingxing Zhang, Heinz Maier-Leibnitz Zentrum (MLZ), Technical University of Munich, Lichtenbergstrasse 1, 85748, Garching, Germany.
Email: xingxing.zhang@frm2.tum.de

Abstract

Tungsten carbide particles reinforced metal matrix composite (MMC) coatings can significantly improve surface wear resistance owing to their increased surface hardness. However, the presence of macro- and micro-residual stresses in MMC coatings can have detrimental effects, such as reducing service life. In this study, neutron diffraction was used to determine the residual stresses in spherical fused tungsten carbide (sFTC) reinforced Cu matrix composite surface deposits after laser melt injection. We also developed a thermo-mechanical coupled finite element model to predict residual stresses. Our findings reveal that sFTC/Cu composite deposits produced with a preheating temperature of 400°C have low residual stresses, with a maximum tensile residual stress of 98 MPa in the Cu matrix on the top surface. In contrast, the sFTC/bronze (CuAl10Ni5Fe4) composite deposit exhibits very high residual stresses, with a maximum tensile residual stress in the Cu matrix on the top surface reaching 651 MPa. These results provide a better understanding of the magnitudes and distributions of residual stresses in sFTC-reinforced Cu matrix composite surface deposits manufactured via laser melt injection.

KEYWORDS

coating, finite element modelling, metal matrix composite, neutron diffraction, residual stress

1 | INTRODUCTION

Friction and wear cause a loss of 2%–7% of the gross national product in industrialised countries.[1] Therefore, developing wear-resistant coatings and optimising their manufacturing processes are essential.[2–4] Metal matrix composite (MMC) coatings, combining the hardness of the reinforcements and the ductility of the metal matrix, are suitable for improving surface wear resistance.[5] In previous investigations, a novel MMC coating has been developed via laser melt injection over the last few years, which consists of a CuAl10Ni5Fe4 matrix and spherical fused tungsten carbide (sFTC, including WC and W_2C) with content up to $\sim$54 vol%. Tribological tests have shown that the MMC coating can reduce wear by $\sim$80%.[6] However, the performance and service life of this sFTC/metal composite coating strongly depend on the residual stress state.[7–9]

Due to the manufacturing process, both macro- and micro-residual stresses arise in the sFTC/metal composite coating.[10,11] The laser surface processing causes a high-temperature gradient,[12] leading to macro-residual stress (i.e., type I residual stress). Besides, the large misfit in the thermal expansion coefficient between the sFTC particles and metal matrix leads to a high magnitude of micro-residual stress (i.e., type II residual stress) after cooling down from the manufacturing temperature. These residual stresses affect the performance of the sFTC/metal composite coating significantly. Firstly, the release of residual stresses during the service process leads to dimensional distortion of the MMC coating. Secondly, the superposition of residual stresses and applied stress leads to unexpected cracking, reducing the fatigue strength[12] and the MMC coating's service life.[13] Hence, it is critical to characterise the residual stresses in the sFTC/metal composite coating.

In this research, the residual stresses in the laser-processed Cu matrix composite surface deposits were characterised via neutron diffraction experiments. The residual stresses along the depth direction from the surface of the deposit to the centre of the sample can be determined in a nondestructive way due to the large penetration depth of neutrons. A corresponding thermo-mechanical finite element model was developed to predict and explain the temperature and residual stress fields. These investigations can help the researchers to control the residual stresses in the Cu matrix composite surface deposits and increase the service life of wear-resistant coatings in the future.

2 | EXPERIMENTAL

2.1 | Material and laser melt injection

Two types of sFTC/metal composite deposits were studied. The first type is sFTC particles reinforced pure copper (Cu-ETP: electrolytically refined, oxygen-containing copper, hereafter simply called Cu) composite deposit (sFTC/Cu), a model material, which is selected to reduce complexity in residual stress determination by decreasing the number of phases in the composite. The more phases, the more difficult to separate the micro-residual stresses at different locations. The second type is sFTC particles reinforced CuAl10Ni5Fe4 (sFTC/bronze) composite deposit, which is selected to reveal the residual stresses in a typical material used for engineering applications.

The composite deposits were manufactured via laser melt injection (Figure 1a). For producing the sFTC/Cu composite deposit, a TruDisk 2021 laser (Trumpf) with a wavelength of 515 nm was used. The pure copper substrate brick with 50 mm length, 20 mm width and 12 mm height was used. The sFTC particles had particle sizes ranging between 45 and 106 μm and were injected at a powder mass flow of 5 g/min into the melt pool via a discrete coaxial three-jet powder nozzle (Ixun) with a 16 mm working distance. The defocused laser spot diameter was 1.9 mm, and the laser power was 1.8 kW. The process velocity was 150 mm/min. A heating device (G. Maier Elektrotechnik) was employed to preheat the Cu substrate to 400°C before the laser process. The temperature of the heating device was kept constant during the laser process. Our preliminary experiments confirmed that without preheating, it was not possible to manufacture this sFTC/Cu composite layer. A small layer made of three overlapping laser tracks was produced with a track length of 40 mm. For comparison, the pure Cu bricks were also processed with the same manufacturing conditions without adding sFTC particles, which are called re-melted Cu samples. More manufacturing details can be found in our previous publication.[14]

For producing the sFTC/bronze composite deposit, a TruDisk 12002 laser (Trumpf) with a wavelength of 1030 nm was used. The bronze substrates had the same size as the copper substrates. For laser melt injection of the sFTC/bronze composite deposit, a discrete coaxial six-jet powder nozzle (GTV) with a 25 mm working distance was used. The powder mass flow was adjusted to 20 g/min. The defocused laser spot diameter was 3.0 mm, and the laser power was 2.0 kW.
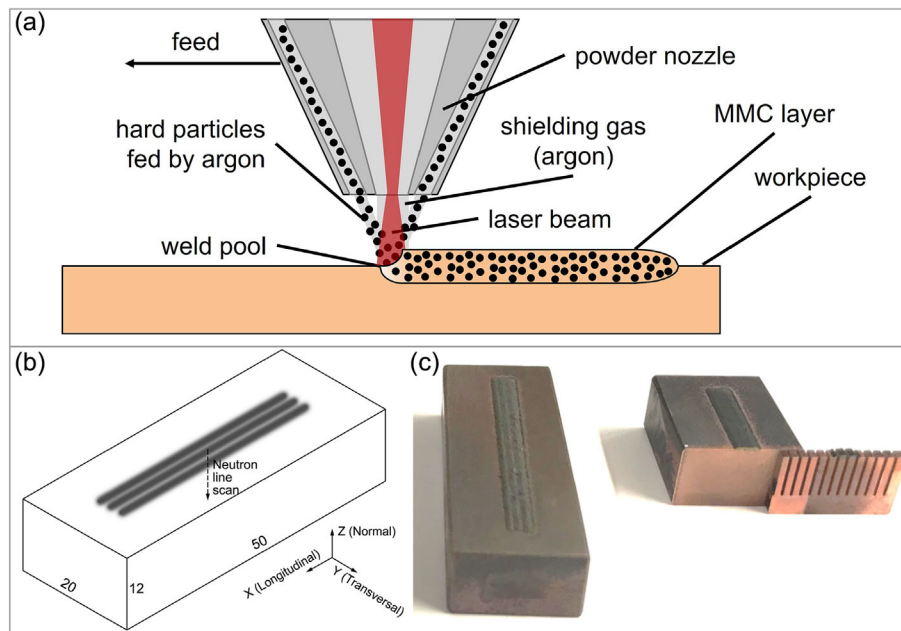
FIGURE 1 The samples: (a) a schematic diagram of manufacturing the samples using a laser melt injection process[16]; (b) the coordinate system for the neutron diffraction scan with the origin at the middle of the centre laser track; (c) the real sFTC/Cu composite deposit brick and the corresponding comb.

The process velocity was 300 mm/min. Different from the sFTC/Cu samples, the bronze substrate was not preheated but fixed on the axis system with a cooled vise. Small layers made of five overlapping laser tracks were manufactured with a track length of 40 mm. In addition, for comparison, corresponding bronze bricks without sFTC particles were laser re-melted with the same process parameters.

Optical microscopy (OM) analysis was carried out on cross-sections of the composite deposits sFTC/Cu and sFTC/bronze as well as on cross-sections of their corresponding re-melted samples. After grinding and polishing the re-melted Cu samples, sFTC/bronze and re-melted bronze samples were etched to visualise the re-melted area and the fusion line. The etching solution consisted of 50 ml water, 50 ml ethanol, 20 ml 37% hydrochloric acid and 5 g $FeCl_3$. Image processing was used to determine the particle content of the composite deposits in MATLAB. Therefore, small regions of interest within the reinforced area were binarized to distinguish between the sFTC particles and the matrix material. From these binarized regions of interest, the particle content was calculated by the quotient of the number of white pixels (sFTC particles) and the total of pixels in this region of interest.

2.2 | Neutron diffraction

The residual strains and stresses in the Cu matrix of the sFTC/Cu composite deposit and the re-melted Cu sample were characterised using neutron diffraction at the beamline HB-2B High Intensity Diffractometer for Residual stress Analysis (HIDRA) of the High Flux Isotope Reactor, Oak Ridge National Laboratory.[15] The neutron wavelength was 1.54 Å with the Si (422) monochromator. The gauge volume of 10.0 (//X, see Figure 1b) × 0.5 × 0.5 mm³ was used for the transversal and normal directions, and that of 1.0 × 4.0 (//Y) × 1.0 mm³ was used for the longitudinal direction.

In contrast, the residual strains and stresses in the Cu matrix of the sFTC/bronze composite deposit and the re-melted bronze samples were measured via neutron diffraction at the beamline SALSA, Institut Laue-Langevin.[17] The neutron wavelength was 1.644 Å with the Si (400) monochromator. The gauge volumes for the longitudinal, transversal, and normal directions are 0.6 × 2.0 (//Y) × 0.6, 10.0 (//X) × 0.6 × 0.6, and 10.0 (//X) × 0.6 × 0.6 mm³, respectively.

Comb samples were prepared for the strain-free reference values. For the sFTC/Cu composite deposit brick, a twin sFTC/Cu composite deposit brick was manufactured using the same conditions. The sFTC/Cu composite deposit comb was then cut from this twin brick using wire-electrode cutting, as shown in Figure 1c. The sFTC/Cu composite deposit

comb was 2 mm thick. The size of each tooth (except the boundary teeth) of the comb was 2 mm thick (//X) × 1 mm wide (//Y) × 8 mm deep (//Z), with an inter-teeth-space width of 0.5 mm. The gauge volume of 1×10 (//Y) $\times 1$ mm^3 was used for the normal direction of the sFTC/Cu composite deposit comb to get the strain-free reference values. Similarly, the sFTC/bronze composite deposit comb was cut from the twin sFTC/bronze composite deposit brick, whose teeth had the same dimension as the sFTC/Cu composite deposit comb. The gauge volume of 10 (//X) $\times 0.6 \times 0.6$ mm^3 was used for the normal direction of the sFTC/bronze composite deposit comb to get the strain-free reference values. Note that the macro-residual stress and elastic mismatch residual stress are relieved from the comb samples, while the thermal misfit residual stress due to CTE differences of the phases remains in the comb samples.

For both experiments, the Cu (311) peak was selected for the diffraction analysis. The diffraction elastic modulus and Poisson's ratio of Cu (311) are 122.05 GPa and 0.352, respectively.[18] The residual strains ε_i are calculated by

$$\varepsilon_i = \frac{\sin\theta_0}{\sin\theta_i} - 1, \tag{1}$$

where the subscript i denotes the longitudinal (L), transversal (T), and normal (N) directions, θ_0 is the diffraction angle of the comb sample, and θ_i is the diffraction angle of the brick sample. The residual strains are then transformed into the residual stresses using Hooke's law

$$\begin{cases} \sigma_L = E_{311}[(1+\nu_{311})(1-2\nu_{311})]^{-1}[(1-\nu_{311})\varepsilon_L + \nu_{311}(\varepsilon_T + \varepsilon_N)] \\ \sigma_T = E_{311}[(1+\nu_{311})(1-2\nu_{311})]^{-1}[(1-\nu_{311})\varepsilon_T + \nu_{311}(\varepsilon_L + \varepsilon_N)] \\ \sigma_N = E_{311}[(1+\nu_{311})(1-2\nu_{311})]^{-1}[(1-\nu_{311})\varepsilon_N + \nu_{311}(\varepsilon_L + \varepsilon_T)] \end{cases} \tag{2}$$

where σ_L, σ_T, and σ_N are residual stresses in the L, T, and N directions, respectively; $E_{311} = 122.050$ GPa, and $\nu_{311} = 0.352$ for the Cu (311) peak.[18]

2.3 | Thermo-mechanical coupled finite element modelling

The re-melting process of the pure Cu without injection of sFTC particles was modelled. The commercial software LS-DYNA was used to create a thermo-mechanically coupled finite element model for the re-melting process. The laser effect is modelled with the help of a Goldak moving heat source.[19] As an initial condition for the temperature, the substrate's preheating temperature was considered. Variable convection coefficients on all surfaces were chosen to specify the boundary conditions. In order to minimise the number of unknown parameters that need to be calibrated, heat radiation has not been considered to date but will be considered in future investigations.

3 | RESULTS AND DISCUSSIONS

3.1 | Microstructures

Figure 2 shows an etched cross-section of the analysed sFTC/Cu MMC layer and the corresponding re-melted Cu edge layer. The MMC layer is about 4.2 mm in width. The maximum thickness is about 0.8 mm. The homogenously distributed sFTC particles have an area fraction of about 51%. Due to the high density of the sFTC particle with 16 to 17 g/cm^3, the MMC layer forms at the bottom of the melt pool. Thus, the geometry of the MMC layer follows the geometry of the melt pool, which creates a fluctuating thickness. The corresponding re-melted surface has nearly the same melt pool geometry and size, with 4.5 mm in width and 0.4 mm in depth.

The sFTC/bronze MMC layer shows a very different microstructure, see the etched cross-section in Figure 3. The most prominent characteristics are the larger dimensions. Note the different scale bars in Figure 3. The five tracks sFTC/bronze MMC layer has a width of 18.1 mm and a depth of 1.3 mm. Unlike the sFTC/Cu MMC, the MMC layer in the bronze is much smaller than the melt pool. The MMC thickness is about 0.4 to 0.8 mm, whereas the solidified melt pool is twice the size. Because of the high density of the sFTC particles, the MMC layer is located at the bottom of the melt pool with a hard particle content of about 41%. On top of the MMC layer, there is a hard particle-free zone of
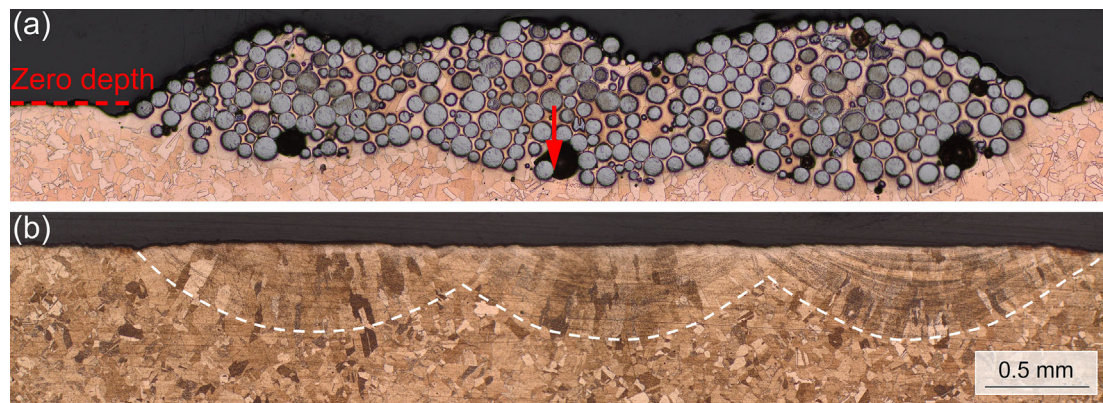
FIGURE 2 Microstructures of multi-track laser processed samples: (a) sFTC/Cu composite deposit and (b) re-melted pure Cu. The zero-depth definition for the sFTC/Cu composite deposit is used in Figure 4, and the red arrow indicates the neutron scan line and direction.
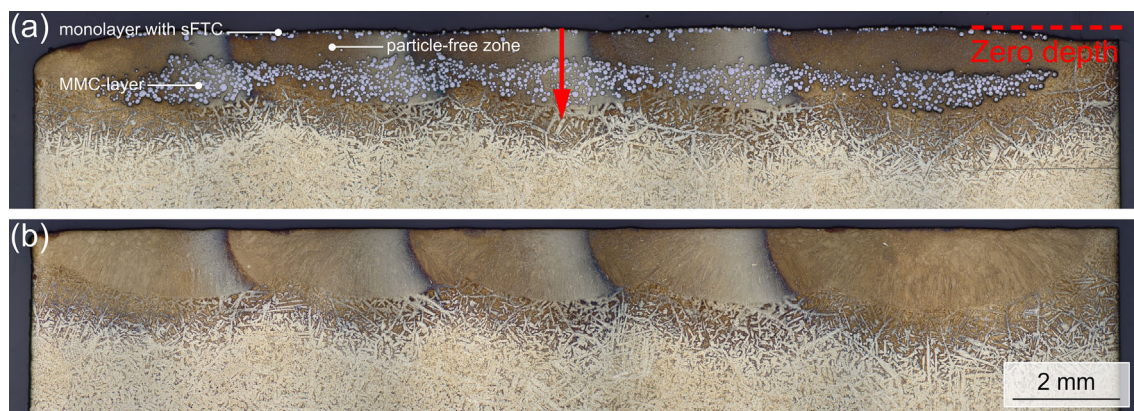

FIGURE 3 Microstructures of multi-track laser processed samples: (a) sFTC/bronze composite deposit and (b) re-melted bronze. The zero-depth definition for the sFTC/bronze composite deposit is used in Figure 6, and the red arrow indicates the neutron scan line and direction.

about 0.6 to 0.8 mm, followed by a discontinuous monolayer of sFTC particles, forming during the last stage of solidification of the melt pool.

3.2 | Residual strains and residual stresses in pure cu-based materials

Figure 4a,b shows the residual strains along the depth direction in the re-melted Cu and the Cu matrix of the sFTC/Cu composite deposit, respectively. Generally, the longitudinal residual strain in the re-melted Cu shows the highest value on the top surface and decreases along the depth direction. Inversely, the transversal and normal residual strains in the re-melted Cu have the lowest values on the top surface and increase along the depth direction. The maximum residual strain magnitudes are $\sim 400 \times 10^{-6}$. In contrast, in the sFTC/Cu composite deposit, all the residual strain components on the surface are tensile, with the maximum transversal residual strain of $\sim 400 \times 10^{-6}$ on the surface. Figure 4c,d shows that in the re-melted Cu, the longitudinal residual stress near the surface is almost zero, while the transversal and normal residual stresses are about compressive 50 MPa on the surface and then increase gradually along the depth direction. Unlike the re-melted Cu case, all residual stress components on the surface show high tensile values. The maximum longitudinal, transversal and normal residual stresses in the Cu matrix of the sFTC/Cu composite deposit on the surface are about 80, 98, and 65 MPa, respectively. The residual stresses decrease gradually until the depth of ~ 1.5 mm.

These results revealed that with a preheating temperature of 400°C, the laser processing generates residual strains and stresses in the pure Cu-based materials within the layer thickness of 2 mm from the top surface. The residual
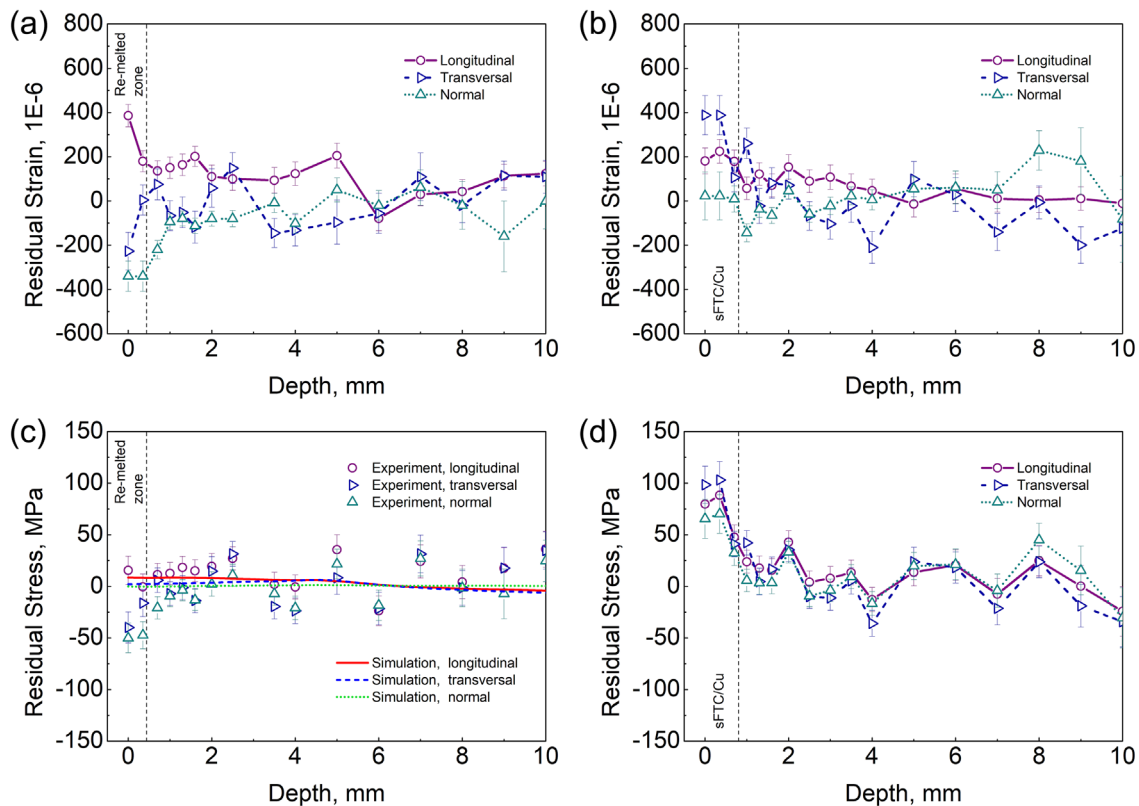
FIGURE 4 Neutron diffraction results of the pure Cu-based materials with three laser tracks: residual strains in (a) the re-melted Cu and (b) the Cu matrix of the sFTC/Cu composite deposit; residual stresses in (c) the re-melted Cu and (d) the Cu matrix of the sFTC/Cu composite deposit. The finite element model simulated residual stress results are also shown in (c) for comparison. The error bars are associated with the fitting errors of the peak positions. Some error bars are longer than others because of the relatively large grain sizes of the Cu matrix, which reduce grain statistics.[20]

strains and stresses below 2 mm fluctuate around the zero level. These residual strains and stresses should be inherited from the initial state before the laser processing. Obviously, the residual strains and stresses in the re-melted Cu are very small. When sFTC hard particles are added, the residual strains and stresses in the Cu matrix of the sFTC/Cu composite deposit increase significantly. Note that the reference values for calculating residual strains and residual stresses were measured from the comb sample cut from the twin sFTC/Cu composite deposit (see Section 2.2). Therefore, the determined residual strains and residual stresses in the Cu matrix only contain the macroscopic residual stress and the microscopic elastic mismatch residual stress, but the microscopic thermal mismatch contribution is not measured here. Here, we observed high tensile residual stress values in the Cu matrix of the sFTC/Cu composite deposit on the surface, and their values are from 65 to 98 MPa.

The maximum temperature predicted by the finite element model is shown in Figure 5a. Heat accumulation towards the end of the processed substrate can be observed. This finding supports experimental studies reporting an increased re-melting depth towards the end of the re-melted zone. It is also noticed that higher temperatures are reached during the re-melting process of the second and third tracks due to further heat accumulation.

The longitudinal residual stress distribution is plotted after cooling to room temperature in Figure 5b. Peak tensile stresses are localised at the starting and ending regions of the re-melting process zone. One reason is that the thermal process is one-sided at these spots. Further, before the laser source started moving, the laser activation was modelled numerically by a linear profile from zero to the chosen laser power within 0.1 s, but the deactivation was instantaneous. On the side surface, it is seen that far from both ends, residual stress varies from tensile stress close to the processed surface to compressive one near the bottom surface. This might be due to the effect of boundary conditions on the bottom surface. The top is heated with a laser resulting in tensile stresses that have to be balanced by compressive ones in other areas to satisfy the balance of momentum.
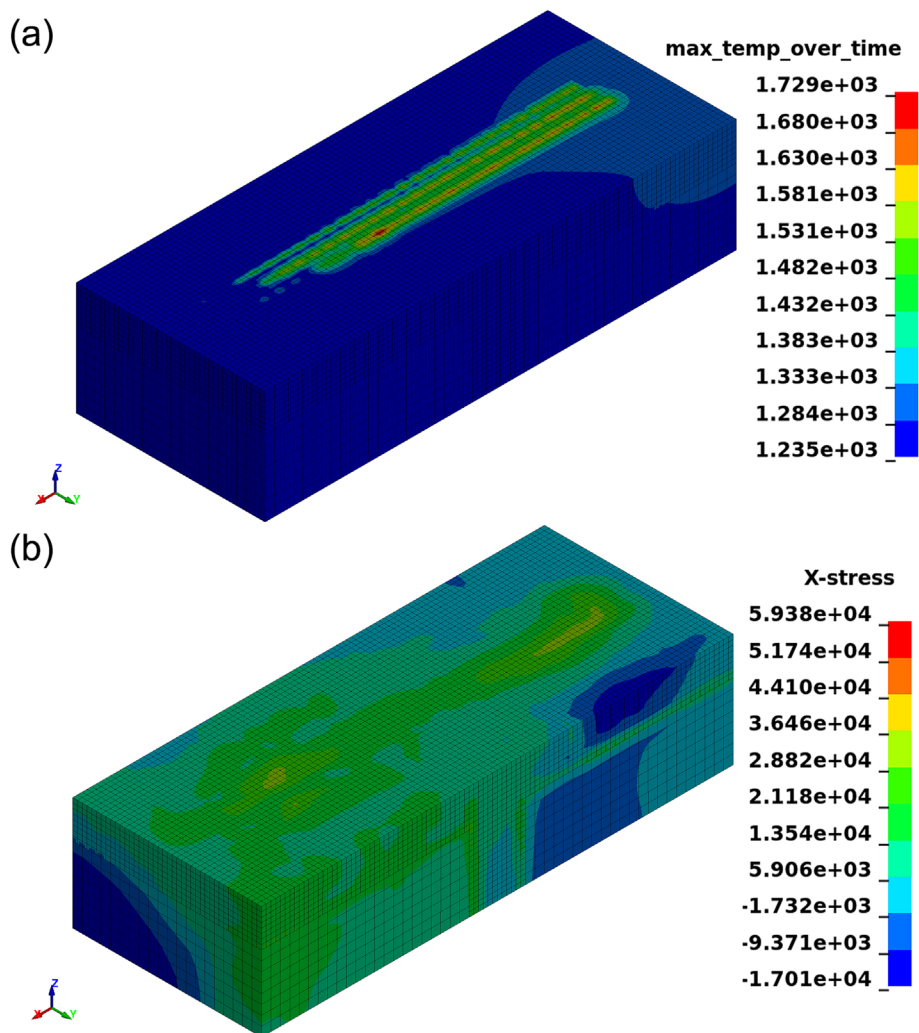
FIGURE 5 Predicted (a) maximum temperature (°C) and (b) longitudinal residual stress (Pa) fields.

3.3 | Residual strains and residual stresses in CuAl10Ni5Fe4 bronze-based materials

Figure 6a shows the residual strains in the Cu matrix of the re-melted bronze, where the longitudinal component has the highest value except the top surface. From the top surface (depth of 0 mm) to 3.2 mm in depth, the longitudinal residual strain increases slightly. The maximum longitudinal residual strain is about 1698×10^{-6} and appears at a depth of 3.2 mm. From 3.2 to 6.2 mm in depth, the longitudinal and transversal residual strains gradually decrease while they increase below 6.2 mm. The variation tendency of the normal residual strain below 3.2 mm is opposite to those of the longitudinal and transversal ones.

The residual strains in the Cu matrix of the sFTC/bronze composite deposit are more complex than those in the re-melted bronze, as shown in Figure 6b. From the top surface to 1.4 mm in depth, both longitudinal and transversal residual strains generally decrease, while the normal component shows an opposite variation tendency. The maximum tensile residual strain appears in the transversal direction and on the top surface, with a value of about $3,053 \times 10^{-6}$. The normal residual strain on the top surface is compressive. The longitudinal and transversal residual strains start to increase from 1.4 to 3.8 mm in depth but then decrease until the depth of 6.8 mm. Below 6.8 mm, the residual strains increase slightly.

The residual stresses in the Cu matrix of the re-melted bronze in the re-melted zone are tensile (Figure 6c). All residual stress components share a similar variation tendency. Local peak values of the longitudinal and transversal residual stresses appear on the top surface, which is 281 and 304 MPa, respectively. All residual stress components increase
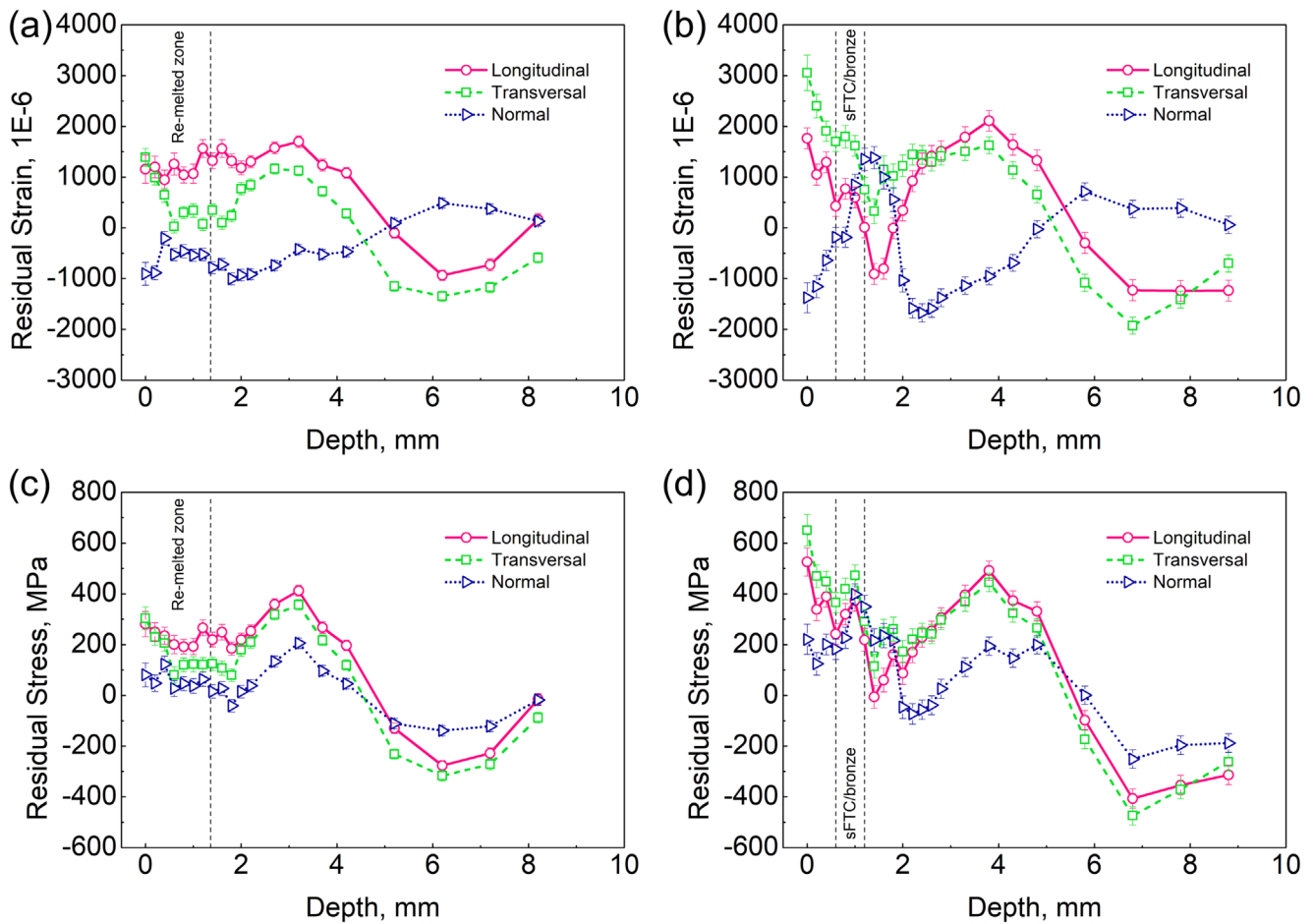
FIGURE 6 Neutron diffraction results of the CuAl10Ni5Fe4 bronze-based materials with five laser tracks: residual strains in the Cu matrix of (a) the re-melted bronze and (b) the sFTC/bronze composite deposit; residual stresses in the Cu matrix of (c) the re-melted bronze and (d) the sFTC/bronze composite deposit. The error bars are related to the fitting errors of peak positions.

below 1.8 mm and reach their maximum values at 3.2 mm in depth. The maximum values of tensile residual stresses are 412, 357 and 206 MPa for the longitudinal, transversal and normal components, respectively. The maximum magnitudes of compressive residual stresses appear at 6.2 mm in depth, with values of −277, −317 and −139 MPa for the longitudinal, transversal and normal components, respectively.

Figure 6d indicates that the residual stresses near the surface zone are significantly higher in the Cu matrix of the sFTC/bronze composite deposit than in the re-melted bronze. The maximum longitudinal and transversal residual stresses appear on the top surface, with values of 525 and 651 MPa, respectively. At ~1.0 mm in depth, that is, the composite layer where the sFTC particles stay (Figure 3), each residual stress component in the Cu matrix shows a local peak, with the values of 374, 473 and 398 MPa for the longitudinal, transversal and normal components, respectively. Besides, an additional local tensile residual stress peak appears at 3.8 mm in depth, with 492, 445 and 194 MPa for the longitudinal, transversal and normal components, respectively. The maximum magnitudes of the compressive residual stresses locate at 6.8 mm in depth, with the values of −406, −473 and −251 MPa for the longitudinal, transversal and normal directions, respectively.

It can be seen that the residual strain and stress levels in the present CuAl10Ni5Fe4 bronze-based materials are significantly higher than those in the pure Cu-based materials. Two reasons should be associated with this phenomenon. On the one hand, the strength of the CuAl10Ni5Fe4 bronze is much higher than that of pure Cu. On the other hand, the high preheating temperature of 400°C used for producing the re-melted Cu and sFTC/Cu composite deposit reduces the thermal gradient dramatically, decreasing the residual strain and stress levels in the pure Cu-based materials.

3.4 | Remarks on the measured residual stresses

As mentioned in Section 3.2, the measured residual strains and stresses in the present sFTC/Cu and sFTC/bronze composite deposits are the macroscopic residual stresses plus the microscopic elastic mismatch residual stresses. The magnitudes and distributions of the measured residual stresses are associated with the following aspects. First of all, like welding processes, the laser-processed tracks experience higher temperatures than the surrounding substrate materials. After cooling, macroscopic tensile residual stresses generate in the laser-processed tracks and heat-affected zones, while macroscopic compressive residual stresses generate in the parent substrates.[21]

Besides, the macro- (not micro-) thermal mismatch between the sFTC reinforced composite track (i.e., sFTC/Cu or sFTC/bronze) and the surrounding substrate material (Cu or bronze) contributes to the macroscopic residual stress. This can be easily understood by the CTE values of different phases. For instance, the CTE values of WC-W$_2$C particle and pure Cu at room temperature are about 9.5×10^{-6} K^{-1}[22] and 17.6×10^{-6} K^{-1},[23] respectively. The CTE of the sFTC/Cu composite layer $\alpha_{\text{sFTC/Cu}}$ might be estimated using the rule of mixture

$$\alpha_{\text{sFTC/Cu}} = V_{\text{sFTC1}}\alpha_{\text{sFTC}} + (1 - V_{\text{sFTC1}})\alpha_{\text{Cu}} \tag{3}$$

where $V_{\text{sFTC1}} = 51\%$. Equation (3) gives $\alpha_{\text{sFTC/Cu}} = 13.5 \times 10^{-6}$ K^{-1}. Therefore, the macroscopic thermal mismatch between the sFTC/Cu composite layer and the surrounding pure Cu substrate is about (17.6–13.5) /17.6 × 100% = 23.3%. Similarly, The CTE of the CuAl10Ni5Fe4 bronze is 16.2×10^{-6} K^{-1}.[23] The CTE of the sFTC/bronze composite layer $\alpha_{\text{sFTC/bronze}}$ might be estimated using

$$\alpha_{\text{sFTC/bronze}} = V_{\text{sFTC2}}\alpha_{\text{sFTC}} + (1 - V_{\text{sFTC2}})\alpha_{\text{bronze}} \tag{4}$$

where $V_{\text{sFTC2}} = 41\%$. Equation (4) also gives $\alpha_{\text{sFTC/bronze}} = 13.5 \times 10^{-6}$ K^{-1}. Therefore, the macroscopic thermal mismatch between the sFTC/bronze composite layer and the surrounding bronze substrate is about 16.7%. After cooling, this macroscopic thermal mismatch effect adds macroscopic compressive residual stresses to the sFTC-reinforced composite tracks because of the smaller effective CTEs and macroscopic tensile residual stresses to the surrounding substrates because of the higher CTEs.

Furthermore, the macro- (not micro-) elastic mismatch between the sFTC reinforced composite track (sFTC/Cu or sFTC/bronze) and the surrounding substrate material (Cu or bronze) also contributes to the macroscopic residual stress. The Young's moduli of WC, W$_2$C, Cu, and CuAl10Ni5Fe4 bronze are 702,[24] 444,[24] 128[23] and 115[23] GPa, respectively. Therefore, the sFTC/Cu and sFTC/bronze composite tracks have much higher effective Young's moduli than their surrounding substrates. This macro-elastic mismatch effect enhances the residual stresses in the composite tracks. Suppose macro-residual stresses in the composite tracks are tensile. In that case, the macro-elastic mismatch effect leads to higher macro-tensile residual stresses in the composite tracks due to the higher effective Young's moduli. This likely is the reason for the tensile residual stress peak at ~1.0 mm in depth for the sFTC/bronze composite deposit (Figure 6d). Note that this macro-elastic mismatch contribution is not the same as the micro-mismatch residual stresses that are mentioned in Section 3.2. The micro-mismatch residual stresses are the micro residual stresses between sFTC particles and Cu or bronze within the sFTC/Cu or sFTC/bronze composite tracks. In contrast, the macro-mismatch residual stresses are the ones between the sFTC/Cu or sFTC/bronze composite track and the surrounding substrates (Cu or bronze).

To summarise, the residual stresses in the sFTC/Cu and sFTC/bronze composite deposits are much more complex than those in the re-melted Cu and bronze. The residual stresses in the composite deposits are caused by the macro-temperature gradient, the macro-thermal mismatch, the macro-elastic mismatch, and also the micro-elastic mismatch effects. Moreover, the composite tracks are not flat but have a wavy shape in the cross-section. Therefore, it is virtually impossible to develop an analytical model to explain the magnitudes and distributions of these residual stresses. A sophisticated finite element model considering the thermo-mechanical coupling effect, the sFTC particles and their distributions are required to develop in the future for predicting these complex residual stresses in the composite deposits.

3.5 | Experimental errors

In this investigation, the gauge volumes used for neutron measurements are small because the composite deposits are thin layers on or near the top surface. Using small gauge volumes could cause experimental errors due to two aspects.

On the one hand, small gauge volumes imply a small number of grains participating in the diffraction event. Therefore, the grain statistics are not as good as when large gauge volumes are employed. This will increase statistical errors.[25] On the other hand, for small gauge volumes, the measurement accuracy becomes more sensitive to the alignment accuracy of the sample position. In addition to the small gauge volumes, the comb samples could also contribute to experimental errors. We assume that the comb samples cut from the twin bricks have the same state as the target bricks. In fact, this is not the real case, especially when the grain number is small. Therefore, deviations of measured strain-free reference values also cause errors.

4 | CONCLUSIONS

1. With a preheating temperature of $400°C$, the laser processing generates residual strains and stresses in the pure Cu-based materials within a layer thickness of about 2 mm from the top surface. The residual stresses in the re-melted Cu substrate are very low. The measured and predicted residual stress results agree with each other. However, adding sFTC particles promotes high tensile residual stresses in the Cu matrix of the sFTC/Cu composite. The residual stresses in the Cu matrix of the sFTC/Cu are tensile and have higher values on the top surface.

2. The residual strains and stresses in the bronze-based materials affect a much thicker layer. In both re-melted bronze and sFTC/bronze, the longitudinal and transversal residual stresses in the Cu matrix are tensile when the depth is smaller than about 5 mm, beyond which they become compressive. In the re-melted bronze, the maximum tensile residual stress appears at a depth of about 3.2 mm. The residual stresses in the Cu matrix of the sFTC/bronze have their largest tensile residual stress on the surface; then, they decrease with increasing depth until the composite layer. The residual stresses in the Cu matrix of the sFTC/bronze composite become higher in the composite layer.

In the present study, residual stresses in the sFTC/Cu and sFTC/bronze composite deposits were determined using neutron diffraction experiments. The results showed very low residual stresses in the re-melted pure Cu with preheating, relating to a reduction in yield strength at higher temperatures. Therefore, future studies may be conducted to examine the impact of preheating. Moreover, the findings can be employed to enhance and validate thermo-mechanical finite element models to forecast residual stresses and improve the performance and lifespan of the composite surface deposits. It is worth noting that microscopic thermal misfit residual stresses were not analysed in this research, and more research will be required to investigate this aspect.

Supported by:

Federal Ministry
for Economic Affairs
and Climate Action

on the basis of a decision
by the German Bundestag

AiF iGF

DVS FORSCHUNG

DATA AVAILABILITY STATEMENT

The data that support the findings of this study are available from the corresponding author upon reasonable request. The data are not publicly available due to privacy or ethical restrictions.

ORCID

Xingxing Zhang https://orcid.org/0000-0002-4616-4524

REFERENCES

[1] P. Dasic, F. Franek, E. Assenova, M. Radovanovic, *Ind. Lubr. Tribol.* **2003**, *55*(6), 287.

[2] E. O. Olakanmi, M. Doyoyo, *J. Therm. Spray Technol.* **2014**, *23*(5), 765.

[3] H. Q. Bai, L. S. Zhong, L. Kang, J. B. Liu, W. J. Zhuang, Z. L. Lv, Y. H. Xu, *J. Alloys Compd.* **2021**, *882*, 160645.

[4] Y. A. Liu, Y. Ding, L. J. Yang, R. L. Sun, T. G. Zhang, X. J. Yang, *J. Manuf. Process.* **2021**, *66*, 341.

[5] W. Zhai, L. Bai, R. Zhou, X. Fan, G. Kang, Y. Liu, K. Zhou, *Adv. Sci.* **2021**, *8*(11), e2003739.

[6] H. Freiße, A. Langebeck, H. Köhler, T. Seefeld, *Dry Met. Forming OAJ.* **2016**, *2*, 001.

[7] N. Srinivasan, L. K. Bhaskar, R. Kumar, S. Baragetti, *Mater. Des.* **2018**, *160*, 303.

[8] R. Ahmed, H. Yu, V. Stoica, L. Edwards, J. R. Santisteban, *Mater. Sci. Eng., a* **2008**, *498*(1–2), 191.

[9] J. Vreeling, *Laser melt injection of ceramic particles in metals*, University of Groningen, Margreet Nieborg **2001**, 142.

[10] P. J. Withers, W. M. Stobbs, O. B. Pedersen, *Acta Metall.* **1989**, *37*(11), 3061.

[11] M. E. Fitzpatrick, M. T. Hutchings, P. J. Withers, *Acta Mater.* **1997**, *45*(12), 4867.

[12] H. Köhler, V. Jayaraman, D. Brosch, F. X. Hutter, T. Seefeld, *Phys. Procedia* **2013**, *41*, 502.

[13] G. A. Webster, A. N. Ezeilo, *Int. J. Fatigue* **2001**, *23*, S375.

[14] A. Langebeck, A. Bohlen, T. Seefeld, X. Zhang, J. R. Kornmeier, M. Hofmann, S. Alameddin, R. P. Alessio, F. Fritzen, *Procedia CIRP* **2022**, *111*, 726.

[15] J. R. Bunn, C. M. Fancher, E. A. Payzant, P. A. Cornwell, W. B. Bailey, R. Gregory, *Rev. Sci. Instrum.* **2023**, *94*, 035101.

[16] T. Pirling, G. Bruno, P. J. Withers, *Residual Stresses VII* **2006**, *524-525*, 217.

[17] P. Warneke, A. Langebeck, A. Bohlen, T. Seefeld, *Mold Die J.* **2022**, *10*, 32.

[18] Y. Zhang, W. Chen, D. L. McDowell, Y. M. Wang, T. Zhu, *J. Mech. Phys. Solids* **2020**, *138*, 103899.

[19] J. A. Goldak, M. Akhlaghi, *Computational welding mechanics*, Springer, New York **2005**.

[20] R. C. Wimpory, R. V. Martins, M. Hofmann, J. R. Kornmeier, S. Moturu, C. Ohms, *Int. J. Pressure Vessels pip.* **2018**, *164*, 80.

[21] P. J. Withers, *Rep. Progr. Phys.* **2007**, *70*(12), 2211.

[22] S. Teslia, I. Solodkyi, O. Yurkova, O. Bezdorozhev, I. Bogomol, P. Loboda, *J. Alloys Compd.* **2022**, *921*, 166042.

[23] J. R. Davis, *ASM specialty handbook: copper and copper alloys*, ASM International, Materials Park, OH **2001**.

[24] H. Taimatsu, S. Sugiyama, Y. Kodaira, *Mater. Trans.* **2008**, *49*(6), 1256.

[25] J. Ahn, E. He, L. Chen, R. C. Wimpory, J. P. Dear, C. M. Davies, *Mater. Des.* **2017**, *115*, 441.